Eigenmode analysis of a high-gain free-electron laser based on a transverse gradient undulator

Panagiotis Baxevanis,[1] Zhirong Huang,[1] Ronald Ruth,[1] and Carl B. Schroeder[2]

[1]*SLAC National Accelerator Laboratory, Menlo Park, California 94025, USA*

[2]*Lawrence Berkeley National Laboratory, Berkeley, California 94720, USA*

(Received 13 October 2014; published 27 January 2015)

The use of a transverse gradient undulator (TGU) is viewed as an attractive option for free-electron lasers (FELs) driven by beams with a large energy spread. By suitably dispersing the electron beam and tilting the undulator poles, the energy spread effect can be substantially mitigated. However, adding the dispersion typically leads to electron beams with large aspect ratios. As a result, the presence of higher-order modes in the FEL radiation can become significant. To investigate this effect, we study the eigenmode properties of a TGU-based, high-gain FEL, using both an analytically-solvable model and a variational technique. Our analysis, which includes the fundamental and the higher-order FEL eigenmodes, can provide an estimate of the mode content for the output radiation. This formalism also enables us to study the trade-off between FEL gain and transverse coherence. Numerical results are presented for a representative soft X-ray, TGU FEL example.

DOI: 10.1103/PhysRevSTAB.18.010701 PACS numbers: 41.60.Cr, 52.65.Ff

I. INTRODUCTION

Using a transverse gradient undulator (TGU) [1–2] in a free electron laser (FEL) is considered a promising approach for those concepts which aim to utilize an electron beam with a relatively large energy spread, such as the beam from a laser-plasma accelerator (LPA) [3–4]. By dispersing the electron beam and canting the undulator poles, both the electron energy and the undulator parameter acquire a linear transverse dependence. A suitable selection of the dispersion and the field gradient minimizes the impact of the energy spread upon the FEL resonance condition, leading to substantially improved gain. On the other hand, a drawback of the TGU is the increased size of the electron beam in the direction of dispersion (typically the horizontal direction). Such an increase in the horizontal size results in a large aspect ratio and provides sufficient transverse space for the higher-order modes to couple efficiently to the beam. Thus, the higher-order growth rates can become comparable to the fundamental, which reduces the transverse coherence of the output FEL radiation. The aim of this paper is to provide a theoretical framework for understanding this effect, which has also been observed in simulations of soft X-ray, TGU-based FELs [3].

As is well known, the operation of a a high-gain FEL can be described in an accurate and self-consistent manner in the context of the Vlasov-Maxwell formalism [5]. This is particularly useful in the linear regime of the interaction, where the solution of the initial value problem can be expressed in terms of the guided eigenmodes of the FEL [6]. In a previous publication [7], we presented a Vlasov-Maxwell theory for a TGU FEL and studied the properties of the fundamental eigenmode through a variational technique, being mostly concerned with gain length optimization studies. Here, we seek to extend our analysis to the higher-order FEL modes. In particular, the present paper is organized as follows: Sec. II contains the main theoretical results. Starting from the mode equation already derived in [7], we introduce a convenient scaling which also highlights the influence of the various effects (diffraction, energy spread, detuning, etc.) upon the mode growth rate and profile. Next, we develop a simplified model which is valid when the radiation size is smaller than the electron beam size. This model admits exact analytical solutions, which allows us to fully determine the mode properties even for arbitrary mode order. These analytical solutions, valuable in their own right, are also quite useful in facilitating the proper choice of variational trial functions for the fundamental and the first few higher-order modes. Making use of this combination of exact and variational solutions, we can obtain the spectrum of the FEL growth rates, identify the modes that are important for a given configuration and provide an estimate of the degree of transverse coherence. Relevant numerical results are given in Sec. III, using the parameters of an LPA-driven, soft X-ray TGU FEL as an example. The principal conclusions and results of this study are summarised in Sec. IV.

II. THEORY

To begin with, we point out that the development to be presented here relies considerably on many of the theoretical results derived in [7]. We shall merely state these results and use them as the starting point for our treatment, referring the reader to our earlier paper for more details. As has already been mentioned, our study is based on an analysis of the eigenmodes of the FEL, i.e., the solutions of the form $A(\mathbf{x})e^{i\mu z}$ for the amplitude of the radiation field (where $\mathbf{x} = (x, y)$ is the transverse position vector and z is the position along the undulator). Each FEL eigenmode is thus characterized by a z-invariant transverse profile $A(\mathbf{x})$ and a constant, complex growth rate μ. As has been shown in [7] for a TGU FEL driven by a Gaussian beam, when the emittance and focusing effects in both transverse dimensions are negligible (the so-called parallel beam case), the equation satisfied by the profile and the growth rate of a growing mode (i.e., one with $\mathrm{Im}(\mu) < 0$) is

$$\left(\mu - \frac{\nabla_\perp^2}{2k_r}\right)A(\mathbf{x}) = U(\mathbf{x}, \mu)A(\mathbf{x}), \tag{1}$$

where

$$U(\mathbf{x}, \mu) = -8\rho_T^3 k_u^3 \exp\left(-\frac{x^2}{2\sigma_T^2} - \frac{y^2}{2\sigma_y^2}\right) \times \int_{-\infty}^0 d\xi \xi e^{i(\mu - \Delta\nu k_u)\xi} e^{-2(\sigma_\delta^{ef})^2 k_u^2 \xi^2} \times \exp\left(-2ik_u C_p \frac{x}{\eta}\xi\right). \tag{2}$$

Here, $\nabla_\perp^2 = \partial^2/\partial\mathbf{x}^2 = \partial^2/\partial x^2 + \partial^2/\partial y^2$ is the transverse Laplacian, $k_r = 2\pi/\lambda_r$ and $k_u = 2\pi/\lambda_u$—where λ_r is the resonant wavelength and λ_u is the undulator period-$\Delta\nu$ is a dimensionless detuning variable while σ_T and σ_y are the rms electron beam sizes in the x and y directions. The former of the last two parameters includes the contribution of the constant dispersion η and is given by $\sigma_T = (\sigma_x^2 + \eta^2\sigma_\delta^2)^{1/2}$, where σ_x is the nondispersive horizontal beam size and σ_δ is the rms energy spread. Moreover, ρ_T and σ_δ^{ef} are, respectively, the effective Pierce parameter and energy spread of the FEL, quantities that are expressed by $\rho_T = \rho(1 + \eta^2\sigma_\delta^2/\sigma_x^2)^{-1/6}$ and $\sigma_\delta^{ef} = \sigma_\delta(1 + \eta^2\sigma_\delta^2/\sigma_x^2)^{-1/2}$, where ρ is the Pierce parameter for $\eta = 0$. The nondispersive FEL parameter is in turn given by $\rho = (K_0^2[JJ]^2 I_p/(16 I_A \gamma_0^3 \sigma_x \sigma_y k_u^2))^{1/3}$, where γ_0 is the average electron energy in units of its rest mass m_0c^2, K_0 is the on-axis undulator parameter, $[JJ] = J_0(K_0^2/(4 + 2K_0^2)) - J_1(K_0^2/(4 + 2K_0^2))$, $I_A \approx 17$ kA is the Alfven current and I_p is the peak current of the electron beam. On the other hand, $C_p = \sigma_x^2/\sigma_T^2 + \bar{\alpha}\eta - 1 = \bar{\alpha}\eta - \eta^2\sigma_\delta^2/\sigma_T^2$ with $\bar{\alpha} = K_0^2\alpha/(2 + K_0^2)$, α being the transverse gradient of the undulator field. Finally, we should also note that the expression for C_p given above is a generalization of the one contained in [7], which only covered the case with $\bar{\alpha} = 1/\eta$. The latter is usually referred to as the TGU resonance condition.

To proceed further, we introduce the scaled quantities $\hat{x} = x/\sigma_T$, $\hat{y} = y/\sigma_y$, $\hat{\mu} = \mu/(2\rho_T k_u)$, $\hat{\xi} = 2\rho_T k_u \xi$, $\hat{\nu} = \Delta\nu/(2\rho_T)$ and $\hat{\sigma}_\delta^{ef} = \sigma_\delta^{ef}/\rho_T$, in which case the eigenmode equation is cast into a fully dimensionless form:

$$\left(\hat{\mu} - p_{dx}\frac{\partial^2}{\partial\hat{x}^2} - p_{dy}\frac{\partial^2}{\partial\hat{y}^2}\right)A(\hat{\mathbf{x}}) = \hat{U}(\hat{\mathbf{x}}, \hat{\mu})A(\hat{\mathbf{x}}), \tag{3}$$

where $\hat{\mathbf{x}} = (\hat{x}, \hat{y})$, $p_{dx} = (4\rho_T k_u k_r \sigma_T^2)^{-1}$ and $p_{dy} = (4\rho_T k_u k_r \sigma_y^2)^{-1}$ are the diffraction parameters (defined in a way analogous to [8]),

$$\hat{U}(\hat{\mathbf{x}}, \hat{\mu}) = -\exp\left(-\frac{\hat{x}^2}{2} - \frac{\hat{y}^2}{2}\right) \times \int_{-\infty}^0 d\hat{\xi}\, \hat{\xi}\, e^{i(\hat{\mu} - \hat{\nu})\hat{\xi}} e^{-(\hat{\sigma}_\delta^{ef})^2\hat{\xi}^2/2} e^{-2i\hat{p}_0\hat{\xi}\hat{x}} \tag{4}$$

and

$$\hat{p}_0 = \frac{\sigma_T}{2\rho_T}\frac{C_p}{\eta} = \frac{\sigma_T}{2\rho_T}\left(\bar{\alpha} - \frac{\eta\sigma_\delta^2}{\sigma_T^2}\right) \tag{5}$$

is a scaled TGU resonance factor. From a physical point of view, $\hat{p}_0 \sim (\Delta\lambda/\lambda_r)_{TGU}/\rho_T$, where $(\Delta\lambda/\lambda_r)_{TGU} \approx (\bar{\alpha}\eta - 1)\sigma_T/\eta$ is the typical wavelength spread due to the transverse gradient and the dispersion. By inspecting Eqs. (3)–(4), an interesting property of the FEL modes can be deduced: if $A(\hat{x}, \hat{y})$ and $\hat{\mu}$ is the mode profile and the growth rate for a given value of $\hat{p}_0$, then $A(-\hat{x}, \hat{y})$ and $\hat{\mu}$ are, respectively, the mode profile and growth rate for $-\hat{p}_0$, all other parameters being the same. This implies that the growth rate is an even function of $\hat{p}_0$, i.e., $\hat{\mu}(-\hat{p}_0) = \hat{\mu}(\hat{p}_0)$. We will return to this important result in the next section.

A. Exactly solvable model

For small values of the beam diffraction parameters ($p_{dx}, p_{dy} \ll 1$), the radiation size in both the x and y directions is smaller than the corresponding size of the electron beam (this assertion will be verified later on). Thus, we have $|\hat{x}|, |\hat{y}| \ll 1$ and we can expand the Gaussian term in the right-hand side of Eq. (4) according to

$$\exp\left(-\frac{\hat{x}^2}{2} - \frac{\hat{y}^2}{2}\right) \approx 1 - \frac{\hat{x}^2}{2} - \frac{\hat{y}^2}{2}.$$

Moreover, when $|\hat{p}_0| \ll 1$, the $\hat{\xi}$-integral in the definition of $\hat{U}$ can be approximated by $\hat{I}_0 - 2i\hat{p}_0\hat{I}_1\hat{x} - 2\hat{p}_0^2\hat{I}_2\hat{x}^2$, where

$$\hat{I}_n = \int_{-\infty}^0 d\hat{\xi}\hat{\xi}^{n+1} e^{\Psi} \tag{6}$$

and $\Psi = i(\hat{\mu} - \hat{\nu})\hat{\xi} - (\hat{\sigma}_\delta^{ef})^2\hat{\xi}^2/2$. Thus, by expanding $\hat{U}$ up to second order in $\hat{x}$ and $\hat{y}$, the mode equation is written in a simplified form as

$$\left(\hat{\mu} - p_{dx}\frac{\partial^2}{\partial\hat{x}^2} - p_{dy}\frac{\partial^2}{\partial\hat{y}^2}\right)A(\hat{\mathbf{x}}) = (F_0 + F_1\hat{x} + F_2\hat{x}^2 + G_2\hat{y}^2)A(\hat{\mathbf{x}}), \tag{7}$$

where $F_0 = -\hat{I}_0$, $F_1 = 2i\hat{p}_0\hat{I}_1$, $F_2 = \hat{I}_0/2 + 2\hat{p}_0^2\hat{I}_2$, and $G_2 = \hat{I}_0/2$. The above result resembles the mode equation for an electron beam with a parabolic transverse profile. However, since we have neglected the transverse cutoff that makes the parabolic distribution a physically rigorous one, our simplified model will only be meaningful when the FEL radiation is contained well within the electron beam. On the other hand, its main strength lies in the fact that Eq. (7) admits exact analytical solutions. In order to determine them, we try an ansatz of the form

$$A(\hat{\mathbf{x}}) = P(\hat{x})Q(\hat{y})e^{-\hat{a}_x\hat{x}^2+\hat{b}\,\hat{x}}e^{-\hat{a}_y\hat{y}^2}, \tag{8}$$

the separable character of which is justified by the absence of any coupling between $\hat{x}$ and $\hat{y}$ in Eq. (7). Substituting, we obtain

$$\begin{aligned}\hat{\mu} - p_{dx}\bigg[&\frac{1}{P}\frac{d^2P}{d\hat{x}^2} + 2(\hat{b} - 2\hat{a}_x\hat{x})\frac{1}{P}\frac{dP}{d\hat{x}} + \hat{b}^2 - 2\hat{a}_x \\ &- 4\hat{a}_x\hat{b}\,\hat{x} + 4\hat{a}_x^2\hat{x}^2\bigg] \\ &- p_{dy}\left[\frac{1}{Q}\frac{d^2Q}{d\hat{y}^2} - 4\hat{a}_y\hat{y}\frac{1}{Q}\frac{dQ}{d\hat{y}} - 2\hat{a}_y + 4\hat{a}_y^2\hat{y}^2\right] \\ = F_0 + F_1\hat{x} + F_2\hat{x}^2 + G_2\hat{y}^2.\end{aligned} \tag{9}$$

If we select $-4p_{dx}\hat{a}_x^2 = F_2$, $-4p_{dy}\hat{a}_y^2 = G_2$ and $4p_{dx}\hat{a}_x\hat{b} = F_1$, the above result reduces to

$$\begin{aligned}\hat{\mu} - p_{dx}&\left[\frac{1}{P}\frac{d^2P}{d\hat{x}^2} + 2(\hat{b} - 2\hat{a}_x\hat{x})\frac{1}{P}\frac{dP}{d\hat{x}} + \hat{b}^2 - 2\hat{a}_x\right] \\ - p_{dy}&\left[\frac{1}{Q}\frac{d^2Q}{d\hat{y}^2} - 4\hat{a}_y\hat{y}\frac{1}{Q}\frac{dQ}{d\hat{y}} - 2\hat{a}_y\right] = F_0.\end{aligned} \tag{10}$$

Since the quantity inside the first bracket is a function of $\hat{x}$ only while its counterpart inside the second bracket is a function of $\hat{y}$, both must be equal to constants. Thus, we could write

$$\frac{1}{P}\frac{d^2P}{d\hat{x}^2} + 2(\hat{b} - 2\hat{a}_x\hat{x})\frac{1}{P}\frac{dP}{d\hat{x}} = -4\hat{a}_x m \tag{11}$$

and

$$\frac{1}{Q}\frac{d^2Q}{d\hat{y}^2} - 4\hat{a}_y\hat{y}\frac{1}{Q}\frac{dQ}{d\hat{y}} = -4\hat{a}_y n, \tag{12}$$

where m and n are—at this stage—real numbers. However, the requirement for $A(\hat{\mathbf{x}})$ to be bounded necessitates that m and n be positive integers, i.e., $m, n = 0, 1, 2, 3, \ldots$. In this case, the solutions for P and Q are given by

$$P(\hat{x}) = H_m\{\sqrt{2\hat{a}_x}[\hat{x} - \hat{b}/(2\hat{a}_x)]\} \tag{13}$$

and

$$Q(\hat{y}) = H_n(\sqrt{2\hat{a}_y}\hat{y}), \tag{14}$$

where H_k are the Hermite polynomials, while the dispersion relation is $\hat{\mu} - p_{dx}[\hat{b}^2 - (4m+2)\hat{a}_x] + (4n+2)p_{dy}\hat{a}_y = F_0$. Summarizing, it has been established that the solutions for the mode profiles are given by

$$\begin{aligned}A_{mn}(\hat{\mathbf{x}}) = H_m\{&\sqrt{2\hat{a}_x}[\hat{x} - \hat{b}/(2\hat{a}_x)]\}e^{-\hat{a}_x\hat{x}^2+\hat{b}\,\hat{x}} \\ &\times H_n(\sqrt{2\hat{a}_y}\hat{y})e^{-\hat{a}_y\hat{y}^2},\end{aligned} \tag{15}$$

where m and n are positive integers or zero. The growth rate $\hat{\mu}$ and the mode parameters $\hat{a}_x, \hat{a}_y, \hat{b}$ satisfy the relations

$$\hat{\mu} + p_{dx}[(4m+2)\hat{a}_x - \hat{b}^2] + (4n+2)p_{dy}\hat{a}_y = -\hat{I}_0 \tag{16}$$

and

$$\begin{aligned}\hat{a}_x^2 &= -\frac{\hat{I}_0 + 4\hat{p}_0^2\hat{I}_2}{8p_{dx}}, \\ \hat{a}_x\hat{b} &= \frac{i\hat{p}_0}{2p_{dx}}\hat{I}_1, \\ \hat{a}_y^2 &= -\frac{\hat{I}_0}{8p_{dy}},\end{aligned} \tag{17}$$

where we recall that the $\hat{I}_k$ quantities are functions of $\hat{\mu}$ defined by Eq. (6). In general, the modes described by Eq. (15) are characterized by an asymmetric intensity profile (given by $|A(\hat{\mathbf{x}})|^2$) which is not invariant under the reflection $x \to -x$, though it is still invariant under $y \to -y$. For example, the fundamental mode (for which $m = 0$, $n = 0$) has a Gaussian profile centered at $\hat{x} = \hat{x}_c = \hat{b}_{xr}/(2\hat{a}_{xr}), \hat{y} = 0$ and is characterized by the scaled rms modes sizes $\hat{\sigma}_{rx} = (4\hat{a}_{xr})^{-1/2}$ and $\hat{\sigma}_{ry} = (4\hat{a}_{yr})^{-1/2}$, where $\hat{a}_{xr}, \hat{a}_{yr}, \hat{b}_{xr}$ are, respectively, the real parts of $\hat{a}_x$, $\hat{a}_y$ and $\hat{b}$. In the limit of vanishing effective energy spread ($\hat{\sigma}_\delta^{ef} \to 0$), we can readily show that $\hat{I}_0 = 1/\hat{w}^2$, $\hat{I}_1 = 2i/\hat{w}^3$ and $\hat{I}_2 = -6/\hat{w}^4$, where $\hat{w} = \hat{\mu} - \hat{\nu}$. Moreover, Eq. (17) then yields

$\hat{a}_x = -i(\sqrt{8p_{dx}}\hat{w})^{-1}(1-24\hat{p}_0^2/\hat{w}^2)^{1/2}$, $\hat{a}_y = -i/(\sqrt{8p_{dy}}\hat{w})$ and $\hat{b} = -(8/p_{dx})^{1/2}(i\hat{p}_0/\hat{w}^2)(1-24\hat{p}_0^2/\hat{w}^2)^{-1/2}$ for the mode parameters. These expressions—when substituted back into Eq. (16)—result in the dispersion relation

$$\hat{\mu} - \frac{i}{\sqrt{2}\hat{w}}\left[(2m+1)\sqrt{p_{dx}}\left(1-\frac{24\hat{p}_0^2}{\hat{w}^2}\right)^{1/2} + (2n+1)\sqrt{p_{dy}}\right] + \frac{8\hat{p}_0^2}{\hat{w}^4}\left(1-\frac{24\hat{p}_0^2}{\hat{w}^2}\right)^{-1} = -\frac{1}{\hat{w}^2}. \quad (18)$$

As $p_{dx}, p_{dy}, \hat{p}_0 \to 0$, Eq. (18) reduces to $\hat{\mu} = -1/\hat{w}^2 = -1/(\hat{\mu}-\hat{\nu})^2$, which is the familiar cubic dispersion relation from 1D FEL theory. Furthermore, since the mode parameters scale according to $\hat{a}_x \sim p_{dx}^{-1/2}$, $\hat{a}_y \sim p_{dy}^{-1/2}$, and $\hat{b}/\hat{a}_x \sim \hat{p}_0$, we also have $\hat{\sigma}_{rx} \sim p_{dx}^{1/4}$, $\hat{\sigma}_{ry} \sim p_{dy}^{1/4}$, and $\hat{x}_c \sim \hat{p}_0$ for the fundamental mode. This supports our earlier assumption that the radiation lies within the electron beam for small values of p_{dx}, p_{dy}, and $\hat{p}_0$.

As a final remark, we briefly comment on the dependence of the growth rate upon $\hat{p}_0$. The previously discussed fact that $\hat{\mu}$ is an even function of $\hat{p}_0$ can be readily verified by an inspection of Eq. (18)—or its more general counterpart for $\hat{\sigma}_\delta^{ef} \neq 0$—which is quadratic with respect to $\hat{p}_0$. This suggests that the power growth rate (given by $-2\mathrm{Im}(\mu)$) is stationary at $\hat{p}_0 = 0$. In fact, a simple numerical study verifies that the power growth rate attains a maximum at that point. Thus, in order to optimize the gain, one should choose $\hat{p}_0 = 0$ or, equivalently, $\bar{\alpha}\eta = 1 - \sigma_x^2/\sigma_T^2$. When this condition is satisfied, the modes also become fully symmetric i.e., they regain their invariance under the reflection $x \to -x$. It is essential to point out that the above conclusions are, in fact, a general property of the FEL eigenmodes stemming from the particular structure of Eqs. (3)–(4). Thus, their validity is not merely a feature of the approximate solution presented here. On the other hand, even though the condition for optimum gain is different from the TGU resonance condition $\bar{\alpha}\eta = 1$, the actual increase in the growth rate is typically very small because the TGU operates in a regime where $\sigma_T \gg \sigma_x$.

B. Variational calculation

The analytical results of the previous section where derived as the exact solution to an approximate, simplified model described by Eq. (7). We now employ a different approach, which aims to approximately calculate the growth rates and the profiles of the FEL eigenmodes for the exact model of Eqs. (1)–(2), without resorting to any truncated expansion of the $\hat{U}$ function. The method under consideration is based on a well-established variational technique [8]. In this case, we start by constructing a so-called variational functional, given by

$$\int d^2\hat{\mathbf{x}} A(\hat{\mathbf{x}})\left(\hat{\mu} - p_{dx}\frac{\partial^2}{\partial\hat{x}^2} - p_{dy}\frac{\partial^2}{\partial\hat{y}^2}\right)A(\hat{\mathbf{x}}) = \int d^2\hat{\mathbf{x}} A^2(\hat{\mathbf{x}})\hat{U}(\hat{\mathbf{x}},\hat{\mu}). \quad (19)$$

Given a trial function for the mode profile $A(\hat{\mathbf{x}})$, this functional yields an estimate of the growth rate $\hat{\mu}$. The basic feature of this variational approach is that a first order variation in the mode profile only results in a second order error in the growth rate, a fact which enhances the accuracy of the method. Here, we seek to derive variational solutions for the first few eigenmodes. In order to make a judicious choice of the trial function for a specific mode, we each time try a form which has the same functional dependence on $\hat{x}$ and $\hat{y}$ as the exact solution given by Eq. (15). For example, we select a trial function of the form $A(\hat{\mathbf{x}}) = e^{-\hat{a}_x\hat{x}^2+\hat{b}\,\hat{x}}e^{-\hat{a}_y\hat{y}^2}$ for the fundamental mode while our choice for the 01 mode (i.e., $m=0$ and $n=1$) is $A(\hat{\mathbf{x}}) = \hat{y}e^{-\hat{a}_x\hat{x}^2+\hat{b}\,\hat{x}}e^{-\hat{a}_y\hat{y}^2}$. Substituting these into Eq. (19), we obtain the result

$$F(\hat{a}_x,\hat{a}_y,\hat{b},\hat{\mu}) = \hat{\mu} + p_{dx}\hat{a}_x + p_{dy}\hat{a}_y + \hat{a}_x^{1/2}(\hat{a}_x+1/4)^{-1/2} \times \hat{a}_y^{1/2}(\hat{a}_y+1/4)^{-1/2} \times \int_{-\infty}^0 d\hat{\xi}\,\hat{\xi}\,e^{i(\hat{\mu}-\hat{\nu})\hat{\xi}}e^{-(\hat{\sigma}_\delta^{ef})^2\hat{\xi}^2/2} \times \exp\left[\frac{(\hat{b}-i\hat{p}_0\hat{\xi})^2}{2\hat{a}_x+1/2} - \frac{\hat{b}^2}{2\hat{a}_x}\right] = 0 \quad (20)$$

for the 00 mode and

$$F(\hat{a}_x,\hat{a}_y,\hat{b},\hat{\mu}) = \hat{\mu} + p_{dx}\hat{a}_x + 3p_{dy}\hat{a}_y + \hat{a}_x^{1/2}(\hat{a}_x+1/4)^{-1/2} \times \hat{a}_y^{3/2}(\hat{a}_y+1/4)^{-3/2} \times \int_{-\infty}^0 d\hat{\xi}\,\hat{\xi}\,e^{i(\hat{\mu}-\hat{\nu})\hat{\xi}}e^{-(\hat{\sigma}_\delta^{ef})^2\hat{\xi}^2/2} \times \exp\left[\frac{(\hat{b}-i\hat{p}_0\hat{\xi})^2}{2\hat{a}_x+1/2} - \frac{\hat{b}^2}{2\hat{a}_x}\right] = 0 \quad (21)$$

for the 01 mode. Equation (20) is a scaled—and slightly generalized—version of the variational dispersion relation included in [7]. Using the stationary condition $\partial\hat{\mu}/\partial\hat{a}_x = \partial\hat{\mu}/\partial\hat{a}_y = \partial\hat{\mu}/\partial\hat{b} = 0$, we also obtain the additional relations $\partial F(\hat{a}_x,\hat{a}_y,\hat{b},\hat{\mu})/\partial\hat{a}_x = 0$, $\partial F(\hat{a}_x,\hat{a}_y,\hat{b},\hat{\mu})/\partial\hat{a}_y = 0$ and $\partial F(\hat{a}_x,\hat{a}_y,\hat{b},\hat{\mu})/\partial\hat{b} = 0$. These three derivative relations have to be solved simultaneously along with Eq. (20)/Eq. (21) in order to determine the properties of the 00/01 mode. As far as the 10 mode is concerned ($m=1$, $n=0$), we now use a trial function of the form $A(\hat{\mathbf{x}}) = (\hat{x}+\hat{\lambda})e^{-\hat{a}_x\hat{x}^2+\hat{b}\,\hat{x}}e^{-\hat{a}_y\hat{y}^2}$ while, for the 11 mode, we choose $A(\hat{\mathbf{x}}) = (\hat{x}+\hat{\lambda})\hat{y}e^{-\hat{a}_x\hat{x}^2+\hat{b}\,\hat{x}}e^{-\hat{a}_y\hat{y}^2}$. These manipulations yield the relations

$$F(\hat{a}_x,\hat{a}_y,\hat{b},\hat{\lambda},\hat{\mu}) = (\hat{\mu}+p_{dy}\hat{a}_y)\left[\left(\hat{\lambda}+\frac{\hat{b}}{2\hat{a}_x}\right)^2+\frac{1}{4\hat{a}_x}\right]+p_{dx}\hat{a}_x\left[\left(\hat{\lambda}+\frac{\hat{b}}{2\hat{a}_x}\right)^2+\frac{3}{4\hat{a}_x}\right]$$
$$+\hat{a}_x^{1/2}(\hat{a}_x+1/4)^{-1/2}\hat{a}_y^{1/2}(\hat{a}_y+1/4)^{-1/2}\int_{-\infty}^{0}d\hat{\xi}\,\hat{\xi}\,e^{i(\hat{\mu}-\hat{\nu})\hat{\xi}}e^{-(\hat{\sigma}_\delta^{ef})^2\hat{\xi}^2/2}$$
$$\times\left[\left(\hat{\lambda}+\frac{\hat{b}-i\hat{p}_0\hat{\xi}}{2\hat{a}_x+1/2}\right)^2+\frac{1}{4\hat{a}_x+1}\right]\exp\left[\frac{(\hat{b}-i\hat{p}_0\hat{\xi})^2}{2\hat{a}_x+1/2}-\frac{\hat{b}^2}{2\hat{a}_x}\right]=0 \tag{22}$$

and

$$F(\hat{a}_x,\hat{a}_y,\hat{b},\hat{\lambda},\hat{\mu}) = (\hat{\mu}+3p_{dy}\hat{a}_y)\left[\left(\hat{\lambda}+\frac{\hat{b}}{2\hat{a}_x}\right)^2+\frac{1}{4\hat{a}_x}\right]+p_{dx}\hat{a}_x\left[\left(\hat{\lambda}+\frac{\hat{b}}{2\hat{a}_x}\right)^2+\frac{3}{4\hat{a}_x}\right]$$
$$+\hat{a}_x^{1/2}(\hat{a}_x+1/4)^{-1/2}\hat{a}_y^{3/2}(\hat{a}_y+1/4)^{-3/2}\int_{-\infty}^{0}d\hat{\xi}\,\hat{\xi}\,e^{i(\hat{\mu}-\hat{\nu})\hat{\xi}}e^{-(\hat{\sigma}_\delta^{ef})^2\hat{\xi}^2/2}$$
$$\times\left[\left(\hat{\lambda}+\frac{\hat{b}-i\hat{p}_0\hat{\xi}}{2\hat{a}_x+1/2}\right)^2+\frac{1}{4\hat{a}_x+1}\right]\exp\left[\frac{(\hat{b}-i\hat{p}_0\hat{\xi})^2}{2\hat{a}_x+1/2}-\frac{\hat{b}^2}{2\hat{a}_x}\right]=0, \tag{23}$$

respectively. In this last two cases, the variational solution is completed by the relations $\partial F/\partial\hat{a}_x=\partial F/\partial\hat{a}_y=\partial F/\partial\hat{b}=\partial F/\partial\hat{\lambda}=0$.

III. NUMERICAL RESULTS

The main practical application of the eigenmode analysis presented in the previous section is to facilitate the optimization of a given TGU-based FEL configuration and to provide an estimate of the mode content in the output radiation. The parallel beam formalism developed in this paper is particularly suitable for describing FELs driven by low emittance electron beams, which is often the case for LPA-based concepts [9–10]. An interesting example of such a concept was first discussed in [3] (its parameters are also listed in Table I). It refers to a machine which would utilize a 1 GeV/10 kA LPA beam with the aim of producing radiation within the so-called water window wavelength region (in particular, the resonant wavelength is 3.9 nm). More specifically, this scheme involves a short period, SC undulator with $\lambda_u = 1$ cm and $K_0 = 2$, while the normalized emittance of the LPA beam is as low as 0.1 μm. The listed value for the nondispersive rms beam sizes σ_x and σ_y ($\sim$10 μm) is based on a 2.5 m value for the electron beta functions in the center of the undulator (which is about half the projected undulator length). This results in a ρ value of approximately 6×10^{-3}, which is smaller than the beam energy spread $\sigma_\delta = 0.01$. This raises the possibility of using a TGU to improve the FEL gain. This parameter set was also used in [7] in order to demonstrate the optimization of the dispersion η using a variational calculation for the fundamental FEL mode (for the case with $\bar{\alpha} = 1/\eta$). The main results are summarized in the graph of the frequency-optimized gain length vs the dispersion, which is shown in Fig. 1 (blue curve). In terms of our present scaling, the power gain length L_g is given by

TABLE I. Undulator and electron beam parameters.

Parameter	LPA
Undulator parameter K_0	2
Undulator period λ_u	1 cm
Beam energy $\gamma_0 m_0 c^2$	1 GeV
Resonant wavelength λ_r	3.9 nm
Peak current I_p	10 kA
Energy spread σ_δ	10^{-2}
Normalized emittance $\gamma_0\epsilon_x$	0.1 μm
Normalized emittance $\gamma_0\epsilon_y$	0.1 μm
Horizontal size σ_x	11.3 μm
Vertical size σ_y	11.3 μm
FEL parameter ρ	6×10^{-3}

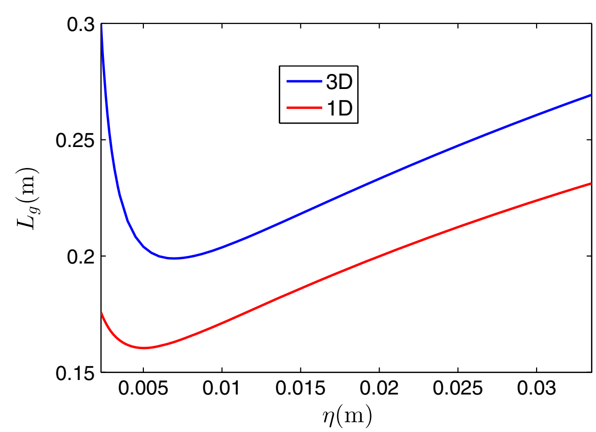

FIG. 1. Frequency-optimized gain length of the fundamental mode as a function of the dispersion for the LPA parameters. The data shown were obtained using the variational solution (blue) and the 1D fitting formula mentioned in the text (red).

$L_g = -\sqrt{3}L_T/(2\mathrm{Im}(\hat{\mu}))$, where $L_T = \lambda_u/(4\pi\sqrt{3}\rho_T)$. The optimization scenario involves varying the dispersion while keeping the other parameters fixed (except, of course, the TGU gradient, which satisfies the condition $\bar{\alpha} = 1/\eta$) and maximizing the power growth rate with respect to the detuning for each dispersion value. Also included are gain length values based on the 1D formula $L_g = L_T[1 + (\hat{\sigma}_\delta^{ef}/\rho_T)^2]$ (red curve). Introduced in [3], the above formula can also be rewritten as

$$L_g = L_0[(\sigma_T/\sigma_x)^{1/3} + (\sigma_\delta/\rho)^2(\sigma_T/\sigma_x)^{-1}], \tag{24}$$

where $L_0 = \lambda_u/(4\pi\sqrt{3}\rho)$. Apart from the obvious increase in the gain length due to the added 3D effects (namely, diffraction), both curves show that there is some optimum value of the dispersion which minimizes the gain length. In the case of the 1D results, this optimum point can be determined analytically. After some manipulation of the fitting formula, we find that the (detuning-optimized) gain length attains a minimum value of

$$L_{g,\min} \approx 1.75 L_0(\sigma_\delta/\rho)^{1/2} \tag{25}$$

when $\sigma_T/\sigma_x \approx 2.28(\sigma_\delta/\rho)^{3/2}$, or, equivalently, when

$$\eta \approx 2.28\sigma_x\sigma_\delta^{1/2}/\rho^{3/2}. \tag{26}$$

These analytical results where first reported in [11], using a slightly different notation. For our LPA parameters, these simple formulas yield an optimum gain length of 16 cm for a 5 mm dispersion. From a physical point of view, the optimum results from balancing the competing influences of the effective FEL parameter and energy spread on the gain length. Specifically, as η—and with it, the horizontal beam size σ_T—increases, ρ_T and $\hat{\sigma}_\delta^{ef}$ both decrease (according to $\sigma_T^{-1/3}$ and σ_T^{-1}, respectively). We note that their ratio also decreases, this time like $\sigma_T^{-2/3}$. Since a decrease in ρ_T ($\hat{\sigma}_\delta^{ef}$) causes L_g to increase (decrease), a stationary point ensues somewhere. For dispersion values smaller than the optimum, the dominant effect is the energy spread ($\hat{\sigma}_\delta^{ef}/\rho_T$ is still rather large), which results in a drastic reduction of L_g with increasing η. On the other hand, for η larger than the optimum, the influence of energy spread becomes smaller and smaller and the variation of L_g is dominated by ρ_T, resulting in a more gradual increase of the gain length. For the 3D results, one needs to also take into account the variation of the diffraction parameters p_{dx} and p_{dy} (they scale like $\sigma_T^{-5/3}$ and $\sigma_T^{1/3}$, respectively) as well as $\hat{p}_0$, which also varies like $\sigma_T^{-5/3}$. Thus, p_{dx} and $\hat{p}_0$ decrease while p_{dy} slowly increases as η is increased, which is why the 3D results do not converge to the 1D values in the limit of large dispersion. In any case, the optimum gain length is now about 20 cm, for a 7 mm dispersion.

In practice, it may actually be desirable to select a dispersion value appreciably larger than the optimum. By thus moving away from the steep part of the optimization curve, the sensitivity of the gain length with respect to variations of η is reduced at a modest cost in terms of FEL gain. However, operating at or to the right side of the optimum typically creates an electron beam with a large ratio of horizontal to vertical size. As has been shown in simulation studies [3], such a configuration can favor the growth of multiple FEL modes in the exponential-gain regime, degrading the transverse coherence of the output radiation. To study this effect from a theory perspective, we first select a dispersion $\eta = 1$ cm (quite close to the optimum) and employ the variational solution in order to ascertain what the ordering of the various FEL modes is with respect to the power growth rate. For this dispersion value, $p_{dx} = 0.008$, $p_{dy} = 0.64$, $\hat{p}_0 = 0.02$ and the e-beam aspect ratio σ_T/σ_y is about 9. The main results are presented in Fig. 2, which shows the negative imaginary part of the scaled growth rate as a function of the detuning for the 00, 10, 01, and 11 modes. For each mode, the power growth rate attains a maximum for some negative detuning value. The corresponding frequency-optimized gain lengths are, respectively, $L_g^{00} = 20.4$ cm, $L_g^{10} = 21.2$ cm, $L_g^{01} = 30.5$ cm, and $L_g^{11} = 32.3$ cm. The other important observation is that modes with the same n-index (and, therefore, similar vertical profiles) form groups with closely spaced growth rates. As expected, most favored are the modes with $n = 0$, which are characterized by Gaussian-like profiles and maximum overlap with the electron beam.

To check whether or not this pattern holds when more higher-order modes are included, we use the truncated, parabolic-like model to obtain equivalent detuning curves

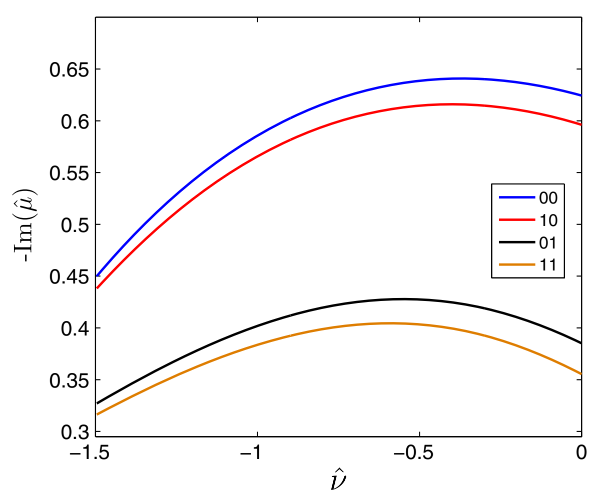

FIG. 2. Negative imaginary part of the FEL growth rate μ (in units of $2\rho_T k_u$) as a function of the detuning $\Delta\nu$ (in units of $2\rho_T$) for various FEL modes (variational data for the $\eta = 1$ cm case).

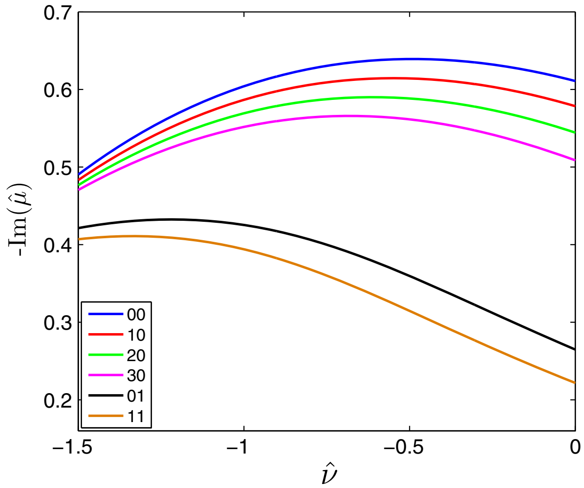

FIG. 3. Negative imaginary part of the FEL growth rate μ (in units of $2\rho_T k_u$) as a function of the detuning $\Delta\nu$ (in units of $2\rho_T$) for several FEL modes (data from the analytical solution, for the $\eta = 1$ cm case).

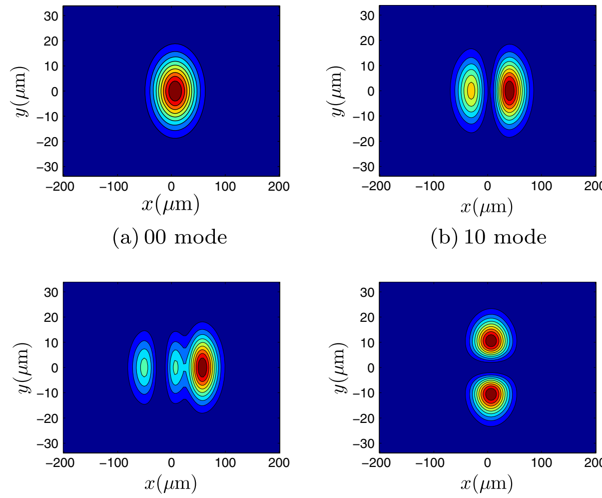

(a) 00 mode (b) 10 mode (c) 20 mode (d) 01 mode

FIG. 4. Mode profiles from the analytical solution ($\eta = 1$ cm). Each profile is calculated for the optimum detuning of the mode. Since $\hat{p}_0 \neq 0$, the intensity profiles are asymmetric in the x-direction.

for the modes already considered plus some additional ones (namely the 20 and 30 modes, see Fig. 3). We note that the data from the analytical solution are not identical to the variational results, as the detuning curves in the former case are shifted towards the left (i.e., the region of negative $\hat{\nu}$). This is due to the fact that, even though p_{dx} and $\hat{p}_0$ are much smaller than unity, p_{dy} is not quite so, with the result that the present parameters probably near the limit of the exact model's applicability. However, we can still verify that the mode spectrum has the same structure as in the variational case. Moreover, even though the detuning curves differ for the two approaches, both the variational and the exact solution actually give very similar estimates for the optimized gain lengths. For comparison, we now obtain $L_g^{00} = 20.4$ cm, $L_g^{10} = 21.2$ cm, $L_g^{20} = 22.1$ cm, $L_g^{30} = 23.1$ cm, $L_g^{01} = 30.2$ cm, and $L_g^{11} = 31.8$ cm. The transverse profiles of some of these modes—calculated for their respective optimized detuning values—are given in Fig. 4.

Our objective is to arrive at a qualitative estimate of transverse coherence from the growth rate data presented above. To begin with, we define the quantities $f_{mn} = \exp(L_{\mathrm{sat}}/L_g^{mn})/\exp(L_{\mathrm{sat}}/L_g^{00})$. These express the ratio of the gain factor for the mn higher-order mode vs that of the fundamental at the saturation length L_{sat}. Since SASE—which is the operating mode assumed here—excites a range of frequencies, all the gain lengths associated with this calculation are optimized with respect to the detuning $\hat{\nu}$. For an estimate of the saturation length, we use the relation $L_{\mathrm{sat}} = N_g L_g^{00}$, where $N_g \approx 20$ or, more precisely, $N_g \approx \log[P_{\mathrm{sat}}/(P_{\mathrm{SASE}}/9)]$, where $P_{\mathrm{sat}} \approx 1.6\rho_T\gamma_0 m_0 c^2 (I_p/e)(L_T/L_g^{00})^2$ is the saturation power and $P_{\mathrm{SASE}} \approx \rho_T^2 \gamma_0 m_0 c^3/\lambda_r$ is the SASE power [12]. For $\eta = 1$ cm, this calculation yields $L_{\mathrm{sat}} \approx 4.4$ m, which agrees with the simulated saturation within a 5 m undulator shown in [3]. Using the values for the mode gain lengths derived via the analytical solution, we obtain $f_{10} \sim 0.43$, $f_{20} \sim 0.19$, $f_{30} \sim 8.5 \times 10^{-2}$, $f_{01} \sim 9.7 \times 10^{-4}$, and $f_{11} \sim 4.7 \times 10^{-4}$. For comparison, the variational values yield $f_{10} \sim 0.43$, $f_{01} \sim 8 \times 10^{-4}$, and $f_{11} \sim 3.6 \times 10^{-4}$. The f_{mn} values—for this as well as subsequent cases—are summarized in Table II. We clarify that when two values are listed in an entry, the first one refers to results from the analytical solution while the second one corresponds to variational data. When only a single value is listed, it only refers to results from the exactly-solvable model. Since the latter approach is the easiest to implement numerically, we focus on that and use the variational method in order to validate its results.

The next step is to consider the total power P_{tot} of the FEL radiation. This quantity can be expressed as

TABLE II. Saturation and transverse coherence parameters (single/first entry refers to data from the exact model while second entry contains variational results).

	$\eta = 4$ mm	$\eta = 1$ cm	$\eta = 2$ cm
σ_T/σ_x	3.7	8.9	17.7
L_g^{00}	21.9/21.5 cm	20.4/20.4 cm	23.3/23.3 cm
L_{sat}	4.5/4.4 m	4.4/4.4 m	5.1/5.1 m
f_{10}	0.04/0.05	0.43/0.43	0.68/0.68
f_{20}	1.4×10^{-3}	0.19	0.47
f_{30}	5.6×10^{-5}	0.085	0.32
f_{01}	$(2.3/2.6) \times 10^{-5}$	$(9.7/8) \times 10^{-4}$	$(2.0/1.7) \times 10^{-3}$
f_{11}	$(1.1/1.3) \times 10^{-6}$	$(4.7/3.6) \times 10^{-4}$	$(1.5/1.2) \times 10^{-3}$
ζ_{coh}	0.78	0.24	0.13

$P_{\rm tot} = \sum_i P_i + \sum_{ij}^{i>j} P_{ij}$, where $P_i = P_i^{(0)} \exp(z/L_i)$ are terms which give the power due to the individual FEL modes—temporarily labeled here by the index i—and $P_{ij} \propto P_{ij}^{(0)} \exp[(z/2)(1/L_i + 1/L_j)]$ are cross terms. Moreover, L_i is the gain length of the ith mode while $P_i^{(0)}$ and $P_{ij}^{(0)}$ are constants. We note that $P_{ij}^{(0)} \neq 0$ unless the ith and jth mode happen to be power-orthogonal. As a measure of transverse coherence, we define the quantity $\zeta_{\rm coh} \equiv P_1/P_{\rm tot}$, which corresponds to the ratio of the power due to the fundamental mode (for which $i = 1$) to the total power. Following [12], we assume that $P_i^{(0)}$ and $P_{ij}^{(0)}$ are all of the same order of magnitude. This is a significant overestimate of the amount of power associated with the higher-order modes but it allows us to simplify the analysis by expressing $\zeta_{\rm coh}$ solely in terms of the gain factor ratios introduced previously. In light of this fact, we expect the resulting estimate of the degree of transverse coherence to be a rather conservative one. A more rigorous approach would require the calculation of the power coefficients through the solution of the initial value problem [13–16]. Given our approximations, we can write $\zeta_{\rm coh} \approx 1/(1+\Delta)$, where $\Delta = \sum_{i>1}(g_i/g_1) + \sum_{ij}^{i>j} \sqrt{g_i/g_1}\sqrt{g_j/g_1}$ and $g_i = e^{z/L_i}$ are the gain factors.

As a specific example, let us assume that we wish to consider only 3 modes, namely 00, 10, and 20. Switching to our previous notation, we have $L_1 \to L_g^{00}$, $L_2 \to L_g^{10}$, $L_3 \to L_g^{20}$, and $z \to L_{\rm sat}$ so $\Delta = f_{10} + f_{20} + f_{10}^{1/2} + f_{20}^{1/2} + f_{10}^{1/2} f_{20}^{1/2}$. Similar expressions can be derived when more modes need to be retained. In our case, we only keep modes of the form $m0$, as it is the members of this group which predominantly determine the transverse coherence (this is justified by the much smaller values of f_{mn} for $n > 0$). For 5 retained modes ($0 \leq m \leq 4$), the data from the analytical solution yield $\zeta_{\rm coh} \sim 0.24$ (this figure remains practically unchanged even when more modes are added). These results would lead us to expect that at least one or two higher-order modes (10 and 20) would be present in the radiation profile at saturation. A pattern similar to the one described above was indeed observed in the TGU simulations of [3] for a 1 cm dispersion.

If we increase the dispersion to 2 cm, the aspect ratio of the electron beam becomes ∼18. The new detuning curves are given in Fig. 5. It is evident that the spacing between modes with the same n-index has decreased. Moreover, the saturation length increases to 5.1 m ($L_g^{00} = 23.3$ cm) and we have $f_{10} \sim 0.68$, $f_{20} \sim 0.47$, $f_{30} \sim 0.32$, $f_{01} \sim 2.0 \times 10^{-3}$, $f_{11} \sim 1.5 \times 10^{-3}$ (analytical data, see Table II), so we expect the transverse coherence to be further degraded. In fact, we obtain $\zeta_{\rm coh} \sim 0.13$. To see if this effect can be mitigated, we next select a dispersion value smaller than the optimum, in particular $\eta = 4$ mm.

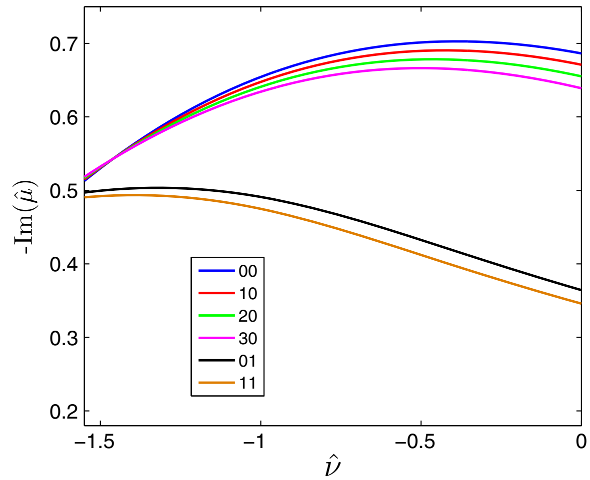

FIG. 5. Negative imaginary part of the scaled FEL growth rate $\hat{\mu}$ as a function of the scaled detuning $\hat{\nu}$ for various FEL modes (data for the $\eta = 2$ cm case, derived from the analytical solution).

The aspect ratio for this reduced dispersion is ∼3.7. This time, the spacing between the modes is clearly larger than before, as can be seen in Fig. 6. Furthermore, we have $L_g^{00} = 21.9$ cm, $L_{\rm sat} = 4.5$ m and the gain factor ratios now satisfy $f_{mn} \leq f_{10} \sim 0.04$, yielding $\zeta_{\rm coh} \sim 0.78$. Thus, it would appear that the transverse coherence of the output radiation could be improved with little loss in terms of gain by choosing a dispersion lower than the optimum value. The drawback is that this places the operating point at the steep part of the optimization curve and may increase the sensitivity of the gain length with respect to η-variations (not to mention technical issues in realizing the stronger TGU gradient).

Using the simpler solution from the parabolic-like model, it is also possible to calculate both the f_{mn}

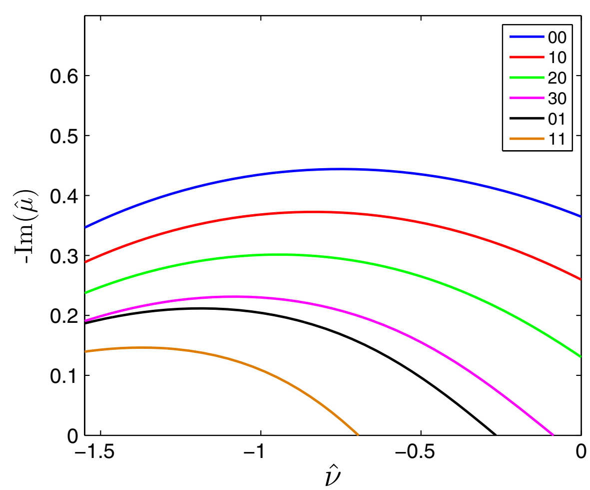

FIG. 6. Negative imaginary part of the scaled FEL growth rate $\hat{\mu}$ as a function of the scaled detuning $\hat{\nu}$ for various FEL modes (data for the $\eta = 4$ mm case, derived from the analytical solution).

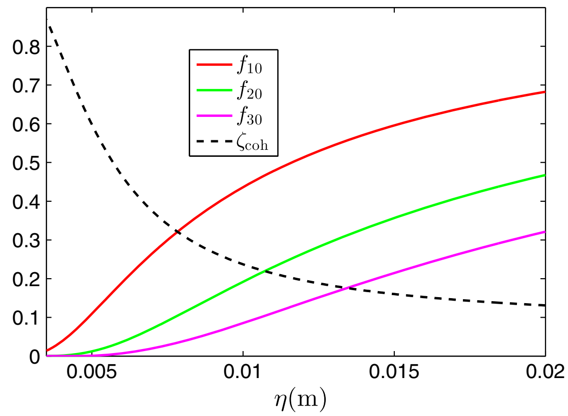

(a) Gain factor ratios and degree of transverse coherence.

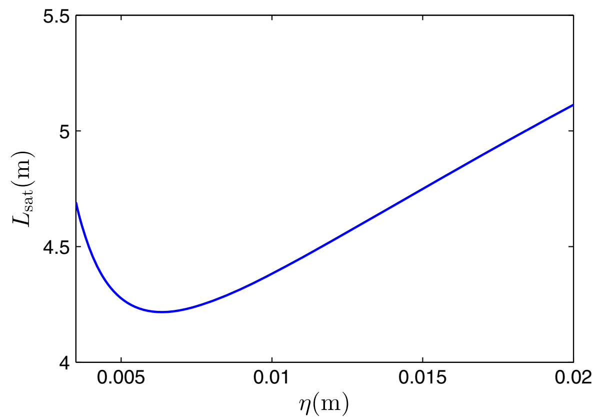

(b) Saturation length.

FIG. 7. Gain factor ratios, degree of transverse coherence (calculated using modes of the form $m0$, with $0 \le m \le 4$) and saturation length as a function of the dispersion (data from the analytical solution).

quantities and ζ_{coh} as continuous functions of the dispersion, which allows us to link the three separated cases discussed above. The results are shown in Fig. 7(a), where the gain ratios for the first few modes with $n = 0$ and the degree of transverse coherence are plotted in terms of η. Again, the observed tendency is that f_{mn} are significantly reduced for smaller dispersion (i.e., smaller aspect ratio), which leads to an improvement in the degree of transverse coherence, as is evident from the substantial increase of ζ_{coh}. The corresponding gain loss is relatively modest (see Fig. 1 or the fundamental gain length values of Table II) while the saturation length exhibits only a weak dependence upon the dispersion [Fig. 7(b)]. As a final remark, we also note that the correlation between radiation mode content and aspect ratio of the electron beam has also been observed in simulations of storage ring-based TGU schemes [17], where making the dispersed beam approximately round caused the output radiation to be dominated by a single, Gaussian-like mode at saturation, resulting in good transverse coherence.

IV. CONCLUSIONS

In this paper, we have developed a theoretical formalism that is suitable for investigating the higher-order mode properties of a TGU-based, high-gain FEL when emittance and focusing effects are negligible (parallel beam regime). We employ a variational approach along with an exactly solvable, parabolic-like model in order to obtain approximate solutions to the eigenmode equation, both for the fundamental and for the higher-order FEL modes. These solutions are then used in a study of the transverse coherence of the radiation from an LPA-based, TGU FEL example. Specifically, using data about the growth rates of the various modes, we arrive at a qualitative estimate of the degree of transverse coherence and study its dependence on the dispersion η. Verifying earlier observations based on simulation, it is established that a stronger TGU gradient (i.e., a smaller dispersion and thus a less excessive horizontal beam size) enhances transverse coherence. Moreover, it is shown that the dispersion that yields the minimum gain length typically also results in a rather degraded transverse coherence. To improve the latter, dispersion values smaller than the optimum may have to be considered. This tradeoff between gain and transverse coherence is likely to be important in determining the operating parameters of a TGU-based FEL.

ACKNOWLEDGMENTS

This work was supported by the Director, Office of Science, of the U.S. Department of Energy under Contracts No. DE-AC02-76SF00515 and No. DE-AC02-05CH11231.

[1] T. Smith, J. M. J. Madey, L. R. Elias, and D. A. G. Deacon, J. Appl. Phys. **50**, 4580 (1979).
[2] N. Kroll, P. Morton, M. Rosenbluth, J. Eckstein, and J. Madey, IEEE J. Quantum Electron. **17**, 1496 (1981).
[3] Z. Huang, Y. Ding, and C. B. Schroeder, Phys. Rev. Lett. **109**, 204801 (2012).
[4] T. Zhang, C. Feng, H. Deng, D. Wang, Z. Dai, and Z. Zhao, Opt. Express **22**, 13880 (2014).
[5] P. Baxevanis, R. Ruth, and Z. Huang, Phys. Rev. ST Accel. Beams **16**, 010705 (2013).
[6] Z. Huang and K.-J. Kim, Phys. Rev. ST Accel. Beams **10**, 034801 (2007).
[7] P. Baxevanis, R. Ruth, Z. Huang, and Y. Ding, Phys. Rev. ST Accel. Beams **17**, 020701 (2014).
[8] M. Xie, Nucl. Instrum. Methods Phys. Res., Sect. A **507**, 450 (2003).
[9] R. Weingartner *et al.*, Phys. Rev. ST Accel. Beams **15**, 111302 (2012).
[10] G. R. Plateau *et al.*, Phys. Rev. Lett. **109**, 064802 (2012).

[11] C. B. Schroeder *et al.*, in *Proceedings of the 35th International Free-Electron Laser Conference, New York, 2013* (JACoW, 2013), http://accelconf.web.cern.ch/AccelConf/FEL2013/.
[12] M. Xie, Nucl. Instrum. Methods Phys. Res., Sect. A **445**, 67 (2000).
[13] L.-H. Yu and S. Krinsky, Phys. Rev. A **35**, 3406 (1987).
[14] E. L. Saldin, E. A. Schneidmiller, and M. V. Yurkov, Opt. Commun. **281**, 4727 (2008).
[15] M. Xie, Nucl. Instrum. Methods Phys. Res., Sect. A **475**, 51 (2001).
[16] Z. Huang and K. J. Kim, Nucl. Instrum. Methods Phys. Res., Sect. A **475**, 59 (2001).
[17] Y. Ding, P. Baxevanis, Y. Cai, Z. Huang, and R. Ruth, in *Proceedings of the 4th International Particle Accelerator Conference, IPAC-2013, Shanghai, China, 2013* (JACoW, Shanghai, China, 2013).